Applied Catalysis B: Environmental 255 (2019) 117748

Contents lists available at ScienceDirect

Applied Catalysis B: Environmental

journal homepage: www.elsevier.com/locate/apcatb

An efficient $Sn_yMn_{1-y}O_x$ composite oxide catalyst for catalytic combustion of vinyl chloride emissions

Wenchao Hua[a], Chuanhui Zhang[b], Yanglong Guo[a,*], Guangtao Chai[a], Chao Wang[b], Yun Guo[a], Li Wang[a], Yunsong Wang[a], Wangcheng Zhan[a,*]

[a] Key Laboratory for Advanced Materials, Research Institute of Industrial Catalysis, School of Chemistry and Molecular Engineering, East China University of Science and Technology, Shanghai 200237, PR China

[b] Institute of Materials for Energy and Environment, College of Materials Science and Engineering, Qingdao University, Qingdao 266071, PR China

ARTICLE INFO

Keywords:
Catalytic combustion
Vinyl chloride
Solid solution
Manganese oxides
Tin oxides

ABSTRACT

A series of $Sn_yMn_{1-y}O_x$ composite oxide catalysts with different Sn/Mn molar ratios (y = 1.0, 0.8, 0.6, 0.3 and 0) were prepared by a co-precipitation method. The catalysts were investigated for the catalytic combustion of vinyl chloride (VC), which is a typical chlorinated volatile organic compound (CVOC). It is found that the existence of Sn-Mn-O solid solution structure over $Sn_yMn_{1-y}O_x$ catalysts can increase the specific surface area and tune the valence state of Mn and the surface properties. As a result, the redox property and the ability of adsorbing oxygen species of $Sn_yMn_{1-y}O_x$ catalysts are enhanced. Meanwhile, more weak and medium acid sites are present on the catalyst surface. Under the synergetic effects of these above-mentioned factors, the catalytic activity of $Sn_yMn_{1-y}O_x$ catalyst for VC oxidation is significantly improved compared with pure SnO_x and MnO_x catalysts. Moreover, the Sn/Mn molar ratio significantly affects the catalytic activity of $Sn_yMn_{1-y}O_x$ catalysts, among which $Sn_{0.6}Mn_{0.4}O_x$ catalyst possesses the best catalytic activity and excellent resistance to Cl poisoning and water-resisting ability. It can retain VC conversion of 100% without any chlorinated byproducts for 100 h at the reaction temperature of 340 °C.

1. Introduction

In the industrial process of polyvinyl chloride (PVC) production, large amounts of emissions containing low concentration of vinyl chloride (VC) are released, which not only seriously pollutes the atmospheric environment, but also does great harm to people's health. Nowadays, several common technologies for removing chlorinated volatile organic compounds (CVOCs) have been proposed, such as physical absorption, direct incineration, biological degradation and catalytic combustion [1]. Compared with other technologies, catalytic combustion is considered as the most economical and promising technology beneficial from the advantages including higher purification efficiency, lower operation temperature and less energy consumption [2–6]. More importantly, these CVOCs with low concentration can be completely oxidized into the harmless products such as CO_2, H_2O, HCl or Cl_2 [7–9]. Therefore, catalytic combustion has attracted more and more attention in the field of CVOCs abatement [10].

During the past periods, numerous catalysts have been investigated for catalytic combustion of CVOCs, mainly focusing on zeolites [11–14], noble metals [10,15] and transition metal oxides [16–18]. In spite of high specific surface areas, variable pore structures and plentiful acid sites of the zeolites, they are sensitive to surface chlorine residual and coke deposition, leading to their poor low-temperature activities and rapid deactivation. Noble metal catalysts always present high catalytic activity for CVOCs abatement. However, their exorbitant price and Cl poisoning remain the main defects and limit the wide applications. Recently, transition metal oxide catalysts have aroused great interests due to their good thermal stability, low cost and adequate catalytic activity for volatile organic compounds (VOCs) abatement. Among all, manganese-based metal oxides have received much attention due to the excellent redox ability [18–20]. However, manganese is sensitive to Cl, and the deposition of Cl will easily occur on the surface of Mn-based catalysts, leading to the catalyst deactivation [21–24]. Therefore, one of the most effective ways to improve the ability to resist chlorine poisoning is to introduce other metals into pure MnO_x through improving the oxygen mobility of pure MnO_x.

SnO_2, as a semiconducting metal oxide, possesses many stable intrinsic defects and oxygen vacancies due to the low formation energies and strong mutual attraction between the tin interstitial and oxygen vacancy [25,26]. As a result, the catalytic activity and thermal stability

* Corresponding authors.
E-mail addresses: ylguo@ecust.edu.cn (Y. Guo), zhanwc@ecust.edu.cn (W. Zhan).

https://doi.org/10.1016/j.apcatb.2019.117748
Received 28 February 2019; Received in revised form 12 May 2019; Accepted 14 May 2019
Available online 16 May 2019
0926-3373/

of transition metal oxide catalysts for CO and CH_4 oxidation can be significantly improved by Sn addition [27–30], as well as H_2O and SO_2 resistance in the long term operation of NH_3-SCR reaction [31–33]. Among transition metals, the ionic radius of Sn^{4+} (0.69 Å for VI coordination) is similar to that of Mn^{3+} (0.65 Å for VI coordination). Thus, Sn and Mn are easy to form solid solution to tune the oxygen mobility of pure MnO_x, and then improve the ability of MnO_x to resist chlorine poisoning. More importantly, Sn has a stronger ability to bond Cl than Mn, due to the higher bond energy (406 KJ·mol^{-1}) of Sn-Cl than that of Mn-Cl (361 KJ·mol^{-1}), which can protect the active species of MnO_x against chlorination. Therefore, the Cl-tolerance of MnO_x can be improved by introducing Sn based on the synergetic effects of the above two factors.

Herein, a series of Sn-Mn composite oxides with different Sn/Mn molar ratios were prepared by a co-precipitation method and investigated as the catalysts for the catalytic combustion of VC. Their physicochemical properties were characterized by numerous techniques including nitrogen sorption, inductively coupled plasma atomic emission spectroscopy (ICP-AES), X-ray diffraction (XRD), X-ray photoelectron spectroscopy (XPS), temperature-programmed reduction of H_2 (H_2-TPR), temperature-programmed desorption of O_2 (O_2-TPD) and temperature-programmed desorption of NH_3 (NH_3-TPD). Finally, a structure-activity relationship was proposed based on the catalyst characterizations and the catalytic activity testing.

2. Experimental

2.1. Catalyst preparation

$Sn_yMn_{1-y}O_x$ (y = 1.0, 0.8, 0.6, 0.3, 0) catalysts were prepared by a conventional co-precipitation method. Procedurally, stoichiometric amounts of $SnCl_4{\cdot}5H_2O$ and 50% $Mn(NO_3)_2$ aqueous solution were dissolved in 150 mL of deionized water, then the ammonia aqueous solution of 6.5 mol/L as the precipitator was added dropwise under stirring until pH reached 9.0. After being aged for 4 h at room temperature, the resultant suspension was filtered and thoroughly washed with deionized water. The obtained sample was dried at 120 °C overnight and then calcined at 550 °C for 4 h in air. The yielded solid materials were grounded, tableted and sieved into 40–60 mesh particles.

2.2. Catalyst characterization

Nitrogen adsorption-desorption isotherms were measured at 77 K on a Micromeritics ASAP 2020 M instrument, and the specific surface area was calculated by Brunauer-Emmett-Teller (BET) method. The chemical compositions of all catalysts were quantitatively determined using inductively coupled plasma atomic emission spectroscopy (ICP-AES) on a flame Perkin Elmer M1100 spectrometer. The powder X-ray diffraction (XRD) patterns of all samples were recorded on a Bruker D8 Focus diffractometer with Cu Kα radiation (40 kV, 40 mA, λ = 1.5406 Å) at a scanning rate of 6°/min.

The X-ray photoelectron spectroscopy (XPS) spectra of all catalysts were recorded on a Thermo ESCALAB 250 spectrometer with a monochromatized AlKα X-ray source (1486.6 eV) and a passing energy of 20 eV. C1 s of adventitious carbon with a binding energy of 284.6 eV was used as the reference.

Temperature-programmed reduction of hydrogen (H_2-TPR) was carried on a P X 200 apparatus (Tianjin Pengxiang Technology Co. Ltd.) using a thermal conductivity detector (TCD). 100 mg of the catalyst was loaded in a quartz reactor in the reduction gas of 5 vol.% H_2/N_2 with a flow rate of 40 mL/min. The reactor was heated from 30 °C to 800 °C at a rate of 10 °C/min, and the signal corresponding to hydrogen consumption was collected by TCD. The amount of H_2 consumption was calibrated by the reduction of CuO.

Temperature-programmed desorption of oxygen (O_2-TPD) was carried out on a Micromeritics Autochem 2920 II instrument. Before testing, 100 mg of the catalyst was pretreated in 3 vol.% O_2/He gas flow of 40 mL/min at 550 °C for 1 h. After cooled down to room temperature, pure He flow of 40 mL/min was introduced into the reactor. And the reactor was heated from room temperature to 800 °C at a rate of 10 °C/min. The signal corresponding to desorbed oxygen was recorded by a Hiden HPR20 mass spectrometer (MS), and the amount of O_2 desorption was calibrated by O_2 pulse.

Temperature-programmed desorption of ammonia (NH_3-TPD) was performed on the same apparatus as H_2-TPR. Typically, 100 mg of the catalyst was pretreated in the nitrogen stream of 50 mL/min at 550 °C for 1 h. After cooling down to 90 °C, ammonia adsorption was performed by introducing a 10 vol.% NH_3/N_2 flow of 50 mL/min and maintained at 90 °C for 0.5 h. Then a N_2 flow of 50 mL/min was switched in order to remove the physically adsorbed ammonia until the stabilization of baseline. Afterwards, the desorption was carried out from 90 °C to 700 °C at a rate of 10 °C /min. The signal corresponding to NH_3 desorption was collected by TCD, and the amount of NH_3 desorption was calibrated by NH_3 pulse.

2.3. Catalyst testing

The catalytic combustion of VC was performed in a continuous flow fixed-bed quartz reactor (I. D. = 6 mm) at atmospheric pressure. The catalyst (400 mg) was packed in the reactor and the activity evaluation was carried out under the reaction conditions of 1000 ppm VC diluted by air and a weight hourly space velocity (WHSV) of 15000 mL·h^{-1} g^{-1}. The height of the catalyst bed was 30 mm. Vinyl chloride was introduced into the reactor using the cylinder gas containing 2 vol.% VC and 98 vol.% N_2. During water resistance testing, a certain amount of water was injected into the dry reaction gas using a syringe pump. The reaction operated from 60 °C to 400 °C in a step model with a 30 min plateau at each reaction temperature. The composition of gas effluent was analyzed by an online PerkinElmer 580 gas chromatograph equipped with a flame ionization detector (FID). The VC conversion was calculated based on the following equation:

$$Xvc(\%) = \frac{[VC]\ in - [VC]out}{[VC]in} \times 100\%$$

3. Characterization and catalytic activity

3.1. N_2 sorption and ICP-AES

The textural properties of all catalysts were firstly measured by N_2 sorption. As shown in Table 1, the surface areas of MnO_x and SnO_x were 24 and 25 m^2 g^{-1}, respectively. With addition of Sn into MnO_x, the surfaces areas of all binary oxides significantly improved. $Sn_{0.6}Mn_{0.4}O_x$ catalyst showed the highest surface area of 108 m^2 g^{-1}. The actual Sn/Mn molar ratios of $Sn_yMn_{1-y}O_x$ were measured by ICP-AES, and the results were also shown in Table 1. All Sn/Mn molar ratios of $Sn_yMn_{1-y}O_x$ were slightly higher than the theoretical values, which may

Table 1
Physicochemical properties of $Sn_yMn_{1-y}O_x$ catalysts.

Catalysts	Sn/Mn molar ratio [a]	S_{BET} [b] ($m^2{\cdot}g^{-1}$)	Crystalline size [c] (nm)	SnO_2 (110) 2θ (°)	SnO_2 (101) 2θ (°)
MnO_x	–	24	49.5	–	–
$Sn_{0.3}Mn_{0.7}O_x$	0.47	78	4.4	26.80	34.24
$Sn_{0.6}Mn_{0.4}O_x$	1.63	108	3.9	26.86	34.33
$Sn_{0.8}Mn_{0.2}O_x$	4.56	66	4.6	26.80	34.12
SnO_x	–	25	16.2	26.61	33.89

[a] Measured by ICP-AES.
[b] Measured by N_2 adsorption (BET method).
[c] Determined and calculated from XRD patterns.

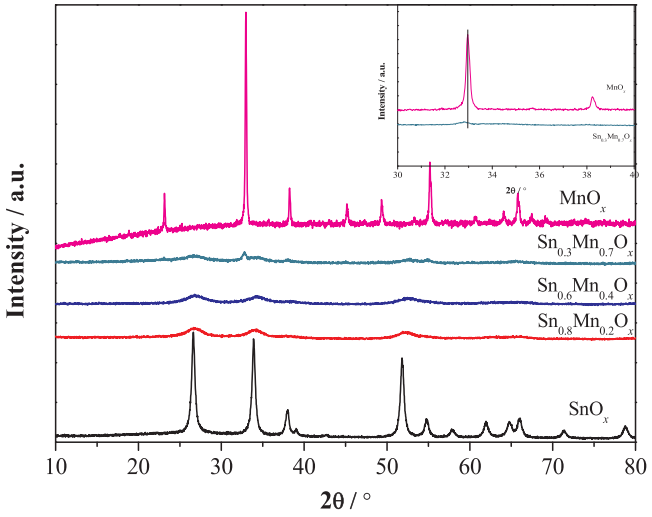

Fig. 1. XRD patterns of $Sn_yMn_{1-y}O_x$ (y = 0, 0.3, 0.6, 0.8 and 1.0) catalysts.

be due to K_{sp} difference between $Sn(OH)_4$ (1.0×10^{-56}) and $Mn(OH)_2$ (1.9×10^{-13}) during the co-precipitation process.

3.2. XRD

The XRD patterns of all catalysts were shown in Fig. 1. Over pure MnO_x, only the diffraction peaks assignable to Mn_2O_3 phase (JCPDS PDF no. 41-1442) [34] could be observed, and its intensity was high, indicating high crystallization of pure MnO_x after calcination. With addition of Sn into MnO_x, the intensity of the diffraction peaks corresponding to Mn_2O_3 significantly decreased over $Sn_{0.3}Mn_{0.7}O_x$ catalyst, and some characteristic diffraction peaks at 2θ = 26.6° and 52.7° corresponding to tetragonal rutile SnO_2 (JCPDS PDF no. 41-1445) could be observed [26]. These results reveal that addition of Sn can remarkably hinder the crystallization of MnO_x, which is consistent with the obvious increase in the surface area of $Sn_{0.3}Mn_{0.7}O_x$ catalyst compared with pure MnO_x. On the other hand, compared with pure MnO_x, the diffraction peaks assignable to Mn_2O_3 over $Sn_{0.3}Mn_{0.7}O_x$ catalyst shifted towards lower angles (insert of Fig. 1). Considering that the ionic radii of Mn^{4+} and Mn^{3+} (0.053 nm for Mn^{4+} and 0.065 nm for Mn^{3+}) were smaller than that of Sn^{4+} (0.069 nm), this phenomenon could be attributed to incorporation of Sn^{4+} into Mn_2O_3 lattice in the form of Sn-Mn-O solid solution matrix [27]. However, presence of the diffraction peaks assignable to SnO_2 indicated that only a certain amount of Sn could be incorporated into Mn_2O_3 lattice.

With the Sn/Mn molar ratio increased to 0.6/0.4, the diffraction peaks corresponding to Mn_2O_3 disappeared completely, while the diffraction peaks assigned to rutile SnO_2 were slightly enhanced. When the Sn/Mn molar ratio further increased to 0.8/0.2, the intensity of the diffraction peaks assigned to rutile SnO_2 hardly changed. To further clarify the structural features of $Sn_yMn_{1-y}O_x$ binary oxides, 2θ values of the two most intensive peaks corresponding to the rutile SnO_2 (110) and (101) phases were comparatively listed in Table 1. Compared with pure SnO_x, both diffraction peaks of SnO_2 over $Sn_yMn_{1-y}O_x$ binary oxides shifted towards higher angles. Considering that the ionic radii of Mn^{4+} and Mn^{3+} were smaller than that of Sn^{4+}, this phenomenon could be attributed to the formation of a Sn-Mn-O solid solution matrix [27]. Furthermore, in terms of the Scherrer equation based on the diffraction peak of SnO_2 (110), it was notable that the crystalline sizes of MnO_x, SnO_x, $Sn_{0.3}Mn_{0.7}O_x$, $Sn_{0.6}Mn_{0.4}O_x$ and $Sn_{0.8}Mn_{0.2}O_x$ catalysts were 49.5, 16.2, 4.4, 3.9 and 4.6 nm, respectively, in which addition of Mn significantly reduced the crystalline sizes of SnO_x (shown in Table 1).

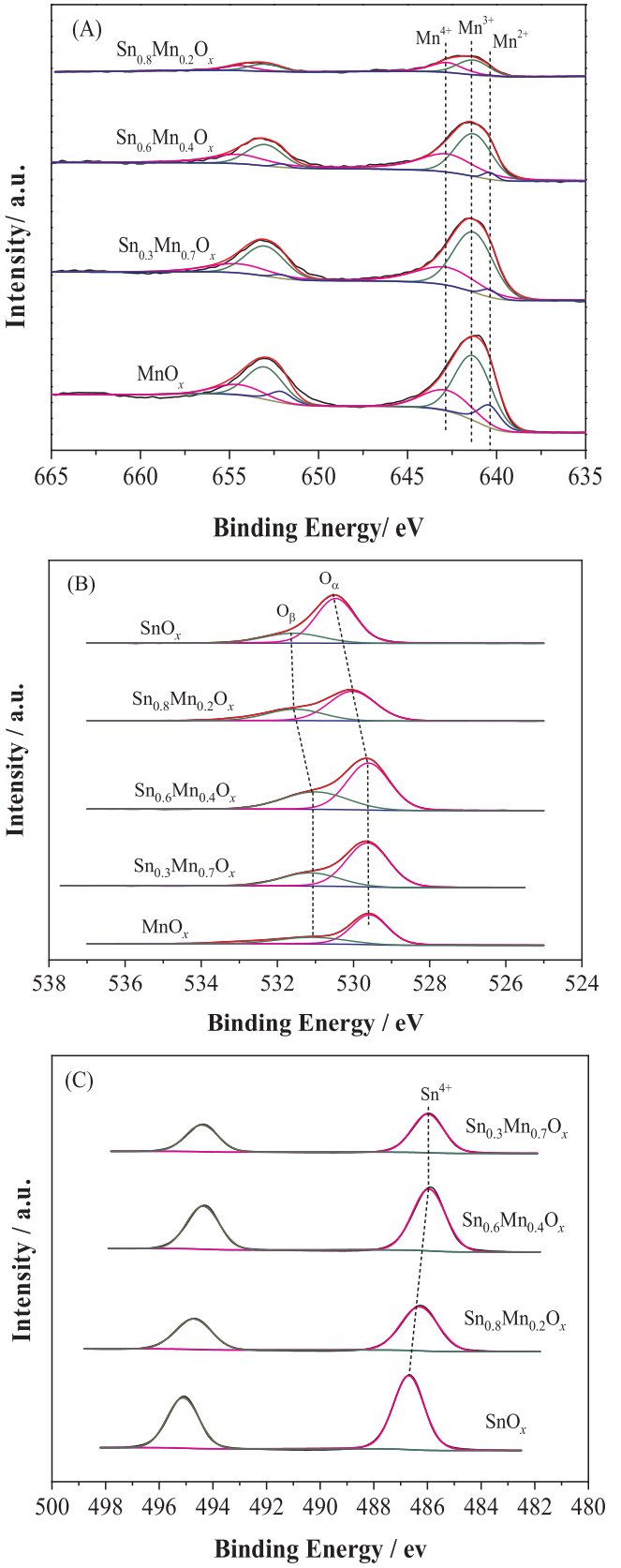

Fig. 2. (A) Mn 2p, (B) O 1s and (C) Sn 3d XPS spectra of $Sn_yMn_{1-y}O_x$ (y = 0, 0.3, 0.6, 0.8 and 1.0) catalysts.

Table 2
Surface compositions and H_2 consumption amounts of $Sn_yMn_{1-y}O_x$ catalysts.

Catalysts	Surface compositions [a]			H_2 consumption /mmol·g^{-1}		
	Mn^{4+}/Mn^{3+}	Mn^{2+}/Mn^{3+}	O_β/O_α	α (T/°C)	β_1 (T/°C)	β_2 (T/°C)
MnO_x	0.43	0.25	0.38	–	2.18 (373)	4.30 (478)
$Sn_{0.3}Mn_{0.7}O_x$	0.53	0.05	0.39	1.29 (252)	0.91 (317)	1.68 (442)
$Sn_{0.6}Mn_{0.4}O_x$	0.86	0.06	0.54	1.38 (263)	0.74 (317)	0.73 (395)
$Sn_{0.8}Mn_{0.2}O_x$	0.88	0.04	0.45	0.65 (267)	0.31 (317)	0.32 (377)
SnO_x			0.31	0.21 (257)		

[a] Determined from XPS results.

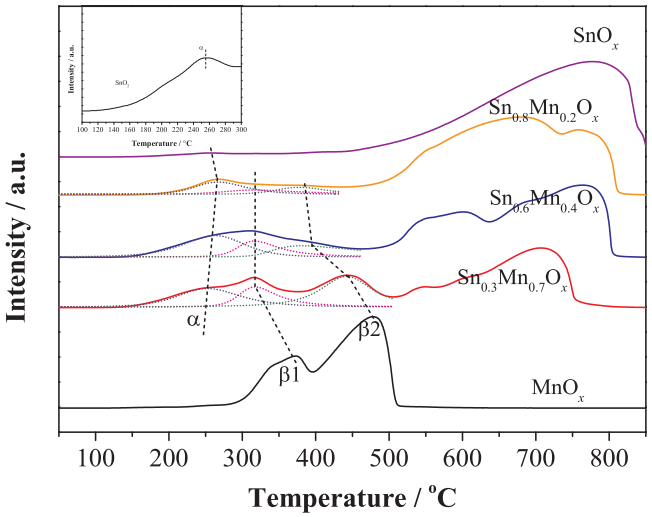

Fig. 3. H_2-TPR profiles of $Sn_yMn_{1-y}O_x$ (y = 0, 0.3, 0.6, 0.8 and 1.0) catalysts.

3.3. XPS

To investigate the surface chemical compositions and the valence states of $Sn_{1-y}Mn_yO_x$ binary oxides, all catalysts were analyzed by XPS technique. Fig. 2(A) shows the Mn 2p spectra of all catalysts. For each catalyst, the asymmetrical Mn $2p_{2/3}$ peak could be deconvoluted into three peaks at the binding energies of 642.8, 641.3 and 640.4 eV, assigned to Mn^{4+}, Mn^{3+} and Mn^{2+} [35–40], respectively. The molar ratios of Mn with different valence states were calculated and listed in Table 2. It could be found that pure MnO_x presented a low Mn^{4+}/Mn^{3+} ratio (0.43) and a high Mn^{2+}/Mn^{3+} (0.25) ratio, which was consistent with the presence of Mn_2O_3 by XRD. When adding Sn into pure MnO_x, the Mn^{4+}/Mn^{3+} ratio increased to 0.53 over $Sn_{0.3}Mn_{0.7}O_x$ catalyst, accompanying with the decrease in the Mn^{2+}/Mn^{3+} ratio (0.05). With an increase in the content of Sn in $Sn_yMn_{1-y}O_x$ catalysts, the Mn^{4+}/Mn^{3+} ratio gradually increased, while the Mn^{2+}/Mn^{3+} ratio almost remained unchanged. It should be specially noted that $Sn_{0.3}Mn_{0.7}O_x$ catalyst possessed a relative lower Mn^{4+}/Mn^{3+} ratio (0.53) than other $Sn_yMn_{1-y}O_x$ catalysts due to the presence of Mn_2O_3, as shown in XRD results.

The O 1s spectra of all catalysts were shown in Fig. 2(B). The asymmetric peak representing multiple types of oxygen species over all catalysts could be deconvoluted into two peaks at 529.6˜530.5 and 531.0˜531.6 eV, assigned to the lattice oxygen species (O^{2-}, denoted as O_α) and surface adsorbed oxygen species (O_2-, O-, O_2^{2-}) or/and some oxygen-containing groups such as OH^- or CO_3^{2-} (denoted as O_β), respectively [35,41,42]. As shown in Table 2, the O_β/O_α ratio of $Sn_{0.3}Mn_{0.7}O_x$ catalyst was 0.39, which was close to that of pure MnO_x. It can be attributed to the Mn_2O_3 phase in $Sn_{0.3}Mn_{0.7}O_x$ catalyst, resulting in the similar surface physicochemical properties to pure MnO_x. However, $Sn_{0.6}Mn_{0.4}O_x$ and $Sn_{0.8}Mn_{0.2}O_x$ catalysts possessed a higher O_β/O_α ratios in comparison with pure SnO_x and MnO_x, indicating that Sn-Mn-O solid solution possessed more surface active oxygen species [28,29]. The O_β/O_α ratios over these catalysts followed a descending order of $Sn_{0.6}Mn_{0.4}O_x$ (0.54) > $Sn_{0.8}Mn_{0.2}O_x$ (0.45) > $Sn_{0.3}Mn_{0.7}O_x$ (0.39) ≈ MnO_x (0.38) > SnO_x (0.31). The highest ratio of O_β/O_α (0.54) of $Sn_{0.6}Mn_{0.4}O_x$ catalyst may be attributed to presence of more Sn-Mn-O solid solutions because of the comparative content of Mn and Sn in the $Sn_{0.6}Mn_{0.4}O_x$ catalyst. In other words, Sn-Mn-O solid solution structure can play an important role as an oxygen donor.

Fig. 2(C) shows the Sn 3d spectra of pure SnO_x and $Sn_yMn_{1-y}O_x$ catalysts. The doublet peaks at 494.4˜495.1 eV and 485.9˜486.7 eV were attributed to Sn $3d_{2/3}$ and $3d_{5/3}$, respectively. The symmetric peaks were all assigned to Sn^{4+} [28,43], indicating that the Sn cations of all catalysts were completely oxidized without any appearance of lower valence states such as Sn^{2+} or metal Sn. Additionally, the peaks of $Sn_yMn_{1-y}O_x$ catalysts shifted to the lower binding energies compared with those of pure SnO_x, indicating the change in chemical environment of Sn cations as a consequence of the formation of Sn-Mn-O solid solution [44].

3.4. H_2-TPR

The H_2-TPR experiments were executed to explore the redox property of $Sn_yMn_{1-y}O_x$ catalysts, and the results were shown in Fig. 3. For pure MnO_x, two reduction peaks centered at 373 °C and 478 °C were observed, which were assigned to reduction of $Mn_2O_3 \rightarrow Mn_3O_4$ (β1) and $Mn_3O_4 \rightarrow$ MnO (β2), respectively [45,46]. Pure SnO_x mainly showed a broad peak in the temperature range of 500–850 °C mainly attributable to reduction of SnO_2 to metallic Sn [47,48]. As for $Sn_yMn_{1-y}O_x$ catalysts, with addition of Sn into MnO_x, two reduction peaks of β1 and β2 significantly shifted to low temperatures due to the formation of Sn-Mn-O solid solution. Furthermore, with an increase in the content of Sn addition, β2 reduction peak gradually shifted to lower temperature, while β1 reduction peak remained unchanged in the temperature. In contrary, the intensity of both β1 and β2 reduction peaks decreased markedly due to the decrease in the content of Mn. The H_2 consumption amounts corresponding to β1 and β2 reduction peaks of the catalysts were calculated and the results are shown in Table 2. With addition of Sn into pure MnO_x, H_2 consumption amounts of both β1 and β2 peaks significantly declined, and further decreased with an increase in Sn content of $Sn_yMn_{1-y}O_x$ catalysts, due to the decrease in Mn content. On the other hand, it is noted that the ratio of H_2 consumption amount between β1 and β2 was about 1/2 over pure MnO_x and $Sn_{0.3}Mn_{0.7}O_x$ catalyst, while it increased to 1/1 over $Sn_{0.6}Mn_{0.4}O_x$ and $Sn_{0.8}Mn_{0.2}O_x$ catalysts due to the increase in the relative content of Mn with high valence state, as shown in XPS results.

Besides the reduction peaks of MnO_x species, a new peak (α peak) appeared at about 260 °C for all $Sn_yMn_{1-y}O_x$ catalysts. Sasikala et al. [47] found that two marked peaks appeared at ˜280 °C and ˜580 °C in the H_2-TPR profiles of weak-crystallized SnO_2 calcined at 300 °C, assigned to the surface and bulk reduction of tetragonal rutile SnO_2, respectively. However, the low-temperature reduction peak disappeared in the H_2-TPR profiles of SnO_2 sample calcined at 800 °C due to the high crystallization [47]. As mentioned in XRD results, $Sn_{0.3}Mn_{0.7}O_x$,

$Sn_{0.6}Mn_{0.4}O_x$ and $Sn_{0.8}Mn_{0.2}O_x$ catalysts were weak-crystallized, owing to the formation of Sn-Mn-O solid solution. Besides, pure SnO_x also showed a weak peak at about 260 °C (insert of Fig. 3). Therefore, the new peak of $Sn_yMn_{1-y}O_x$ catalysts appearing at about 260 °C could be attributed to the surface reduction of tetragonal rutile SnO_2. Moreover, there were multiple reduction peaks over 500 °C, which were assigned to the bulk reduction of tetragonal rutile SnO_2 [47].

In summary, the total H_2 consumption amounts of α and β1 peaks over $Sn_yMn_{1-y}O_x$ catalysts were shown in Table 2, since $Sn_yMn_{1-y}O_x$ catalysts exhibited different catalytic activity for the oxidation of vinyl chloride at the reaction temperature lower than 400 °C. It is following a descending order of $Sn_{0.3}Mn_{0.7}O_x \approx Sn_{0.6}Mn_{0.4}O_x > Sn_{0.8}Mn_{0.2}O_x$, indicating the higher redox property of $Sn_{0.3}Mn_{0.7}O_x$ and $Sn_{0.6}Mn_{0.4}O_x$ catalysts than $Sn_{0.8}Mn_{0.2}O_x$ catalyst. As for pure MnO_x, although the H_2 consumption amount of β1 peak was close to the total H_2 consumption amount of α and β1 peaks over $Sn_{0.3}Mn_{0.7}O_x$ and $Sn_{0.6}Mn_{0.4}O_x$ catalysts, the β1 reduction peak appeared at high temperature, indicating the low redox property.

3.5. O_2-TPD

With an aim to investigate the mobility of surface oxygen species, O_2-TPD measurement was performed and the corresponding results are presented in Fig. 4. Pure MnO_x exhibited an intense peak at 800 °C, assigned to the desorption of bulk lattice oxygen species [49], but no obvious desorption peak was present over pure SnO_x. These results indicated that neither physically adsorbed oxygen nor chemically adsorbed oxygen species existed over pure MnO_x and SnO_x catalysts. Differently, $Sn_yMn_{1-y}O_x$ catalysts exhibited a desorption peak at about 280 °C and two overlapped desorption peaks at the temperature higher than 450 °C. The former was assigned to the desorption of chemically adsorbed oxygen species, while the two latter was assigned to the desorption of bulk lattice oxygen species [8]. Since no chemically adsorbed oxygen species existed over pure MnO_x and SnO_x catalysts, the appearance of chemically adsorbed oxygen species over $Sn_yMn_{1-y}O_x$ catalysts could be attributed to the formation of Sn-Mn-O solid solution. The desorbed amount of chemically adsorbed oxygen species based on the quantitative integration of O_2-TPD profiles are summarized in Table 3. The amount of chemically adsorbed oxygen species over $Sn_yMn_{1-y}O_x$ catalyst increased slightly with an increase in the Sn/Mn molar ratio from 0.3/0.7 to 0.6/0.4. A further increase in the Sn/Mn molar ratio to 0.8/0.2, the amount of chemically adsorbed oxygen species decreased significantly. The amount of chemically adsorbed oxygen species was in the order: $Sn_{0.6}Mn_{0.4}O_x > Sn_{0.3}Mn_{0.7}O_x \gg Sn_{0.8}Mn_{0.2}O_x$, and $Sn_{0.6}Mn_{0.4}O_x$ catalyst possessed the most chemically adsorbed oxygen species. On the other hand, compared to pure MnO_x, the desorption peaks at high temperatures shifted to lower temperatures over $Sn_yMn_{1-y}O_x$ catalysts, indicating the improvement of the lattice oxygen mobility due to the formation of solid-solution structure. In summary, the formation of solid-solution structure of $Sn_yMn_{1-y}O_x$ catalysts can improve the lattice oxygen mobility and produce more chemically adsorbed oxygen species, which is propitious to high catalytic activity of $Sn_yMn_{1-y}O_x$ catalysts for VC oxidation.

Table 3
The desorbed amounts of oxygen and ammonia, and Ea of $Sn_yMn_{1-y}O_x$ catalysts.

Catalysts	O_2 desorption ($mmol \cdot g^{-1}$) [a]	NH_3 desorption ($mmol \cdot g^{-1}$) [b]			Ea (kJ/mol) [c]
		Weak(α)	Medium(β)	Strong(γ)	
MnO_x	–	0.059	0.077	–	71.5
$Sn_{0.3}Mn_{0.7}O_x$	0.0241	0.402	0.220	0.156	55.7
$Sn_{0.6}Mn_{0.4}O_x$	0.0255	0.602	0.282	0.201	49.8
$Sn_{0.8}Mn_{0.2}O_x$	0.0124	0.368	0.204	0.123	79.3
SnO_x	–	–	–	–	124.3

[a] Calculated from O_2-TPD profiles.
[b] Calculated from NH_3-TPD profiles.
[c] Measured within 20% conversion.

3.6. NH_3-TPD

As shown in Fig. 5, the NH_3-TPD profiles of $Sn_yMn_{1-y}O_x$ catalysts can be divided into three counterparts: weak, medium and strong acid sites in different temperature ranges of 100–200 °C, 200–300 °C and > 300 °C. For pure SnO_x, no obvious desorption peak was present in the temperature range of 100–550 °C, which indicated that no acid sites existed over pure SnO_x. In contrary, pure MnO_x showed two weak desorption peaks at 132 and 218 °C, assigned to the desorption of weak and medium acid sites, respectively. With introduction of Sn into pure MnO_x, the two weak desorption peaks became much stronger and overlapped. Besides, a weak desorption peak assigned to the desorption of strong acid sites appeared at high temperature (> 300 °C). It indicates that binary $Sn_yMn_{1-y}O_x$ oxides possess plentiful acid sites, principally weak and medium acid sites, due to the formation of Sn-Mn-O solid solution. The desorbed amount of NH_3 based on the quantitative integration of NH_3-TPD profiles are summarized in Table 3. The amount of desorbed NH_3 increased from $Sn_{0.3}Mn_{0.7}O_x$ to $Sn_{0.6}Mn_{0.4}O_x$ but

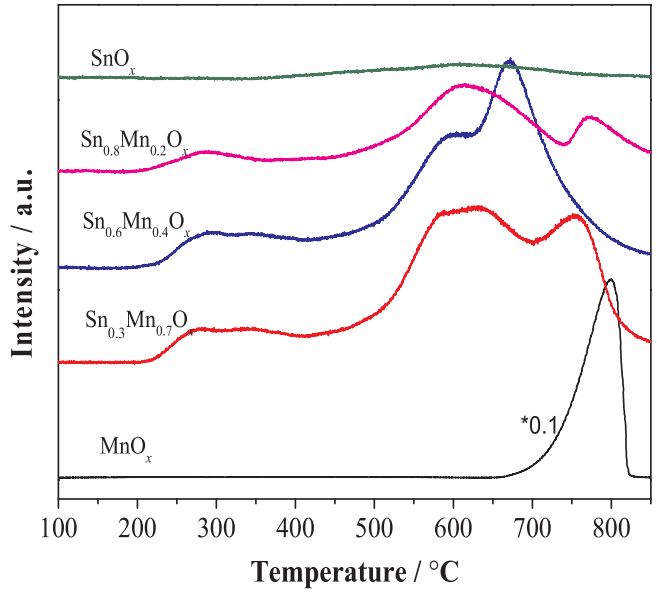

Fig. 4. O_2-TPD profiles of $Sn_yMn_{1-y}O_x$ (y = 0, 0.3, 0.6, 0.8 and 1.0) catalysts.

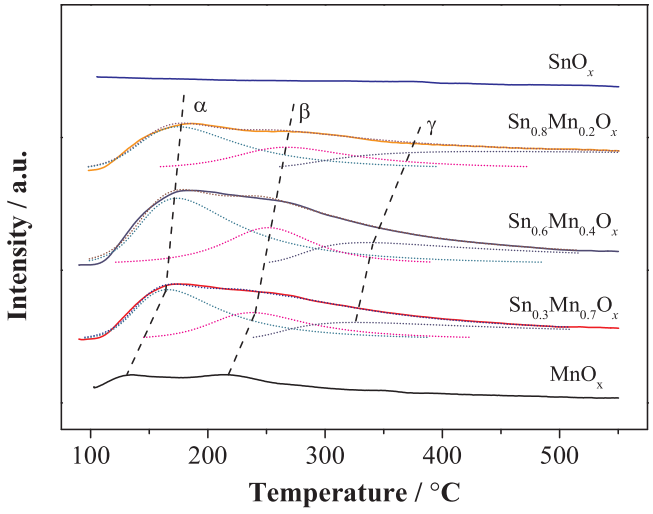

Fig. 5. NH_3-TPD profiles of $Sn_yMn_{1-y}O_x$ (y = 0, 0.3, 0.6, 0.8 and 1.0) catalysts.

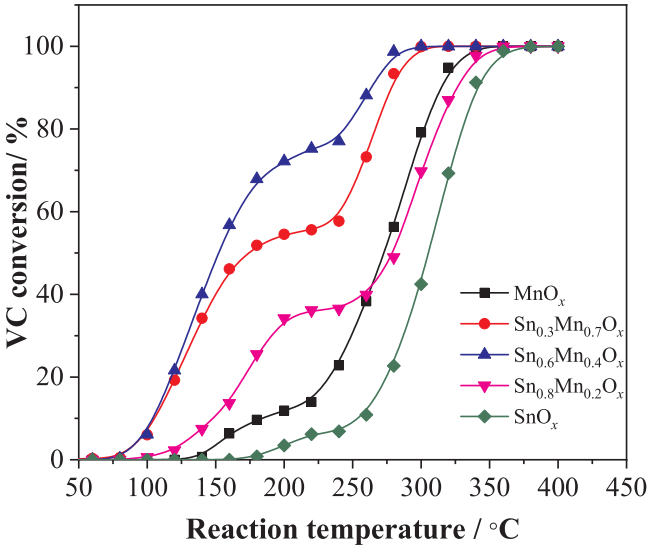

Fig. 6. VC conversion as a function of reaction temperature over $Sn_yMn_{1-y}O_x$ (y = 0, 0.3, 0.6, 0.8 and 1.0) catalysts.

decreased over $Sn_{0.8}Mn_{0.2}O_x$ catalyst. Furthermore, the amount of weak and medium adsorbed NH_3 was in the order: $Sn_{0.6}Mn_{0.4}O_x > Sn_{0.3}Mn_{0.7}O_x > Sn_{0.8}Mn_{0.2}O_x$ » MnO_x. $Sn_{0.6}Mn_{0.4}O_x$ catalyst possesses the most weak and medium acid sites (0.602 mmol/g and 0.282 mmol/g, respectively), which may have positive effects on the adsorption of vinyl chloride, thereby improving the catalytic activity for VC oxidation [50].

3.7. Catalytic activity

The light-off curves of vinyl chloride (VC) conversion as a function of reaction temperature over SnO_x, MnO_x and $Sn_yMn_{1-y}O_x$ catalysts are shown in Fig. 6. Pure SnO_x showed a considerable activity with T_{50} and T_{90} of 305 and 341 °C, respectively. Pure MnO_x possessed a higher activity than pure SnO_x, in which T_{50} and T_{90} decreased to 275 and 315 °C, respectively. With addition of Sn into MnO_x, the catalytic activity of $Sn_yMn_{1-y}O_x$ catalysts significantly improved. Furthermore, the Sn/Mn molar ratio influenced largely the catalytic activity of $Sn_yMn_{1-y}O_x$ catalysts. $Sn_{0.6}Mn_{0.4}O_x$ catalyst exhibited the optimum catalytic activity with T_{50} and T_{90} of 152 and 264 °C, which was 123 and 51 °C lower than those of pure MnO_x, respectively. However, when the Sn/Mn molar ratio increased to 0.8/0.2, the catalytic activity of $Sn_{0.8}Mn_{0.2}O_x$ catalyst decreased markedly, which was close to the catalytic activity of pure MnO_x but still higher than that of pure SnO_2. As shown in Table 3, the corresponding apparent activation energies (E_a) ranked in the order: $Sn_{0.6}Mn_{0.4}O_x$ (49.8 kJ/mol) < $Sn_{0.3}Mn_{0.7}O_x$ (55.7 kJ/mol) < MnO_x (71.5 kJ/mol) < $Sn_{0.8}Mn_{0.2}O_x$ (79.3 kJ/mol) < SnO_x (124.3 kJ/mol). It indicates that introducing appropriate amount of Sn can promote the catalytic activity of MnO_x for VC oxidation.

On the other hand, it is noted that all light-off curves exhibited a step at the reaction temperature range of 175~275 °C, and VC conversion corresponding to the step over different catalysts was dependent on their catalytic activity. The step appeared at VC conversion of 70~80% over $Sn_{0.6}Mn_{0.4}O_x$ catalyst, which was about 40% higher than that over $Sn_{0.8}Mn_{0.2}O_x$ catalyst. The reason was that Cl^- species was gradually accumulated on the catalyst surface and covered the active sites, leading to the temporary deactivation of the catalysts and the presence of a step. When the reaction temperature continued to increase, the accumulated Cl^- species could be converted and VC conversion increased continually. However, the accumulation rate of Cl species was dependent on the catalytic activity of the catalysts, resulting in different

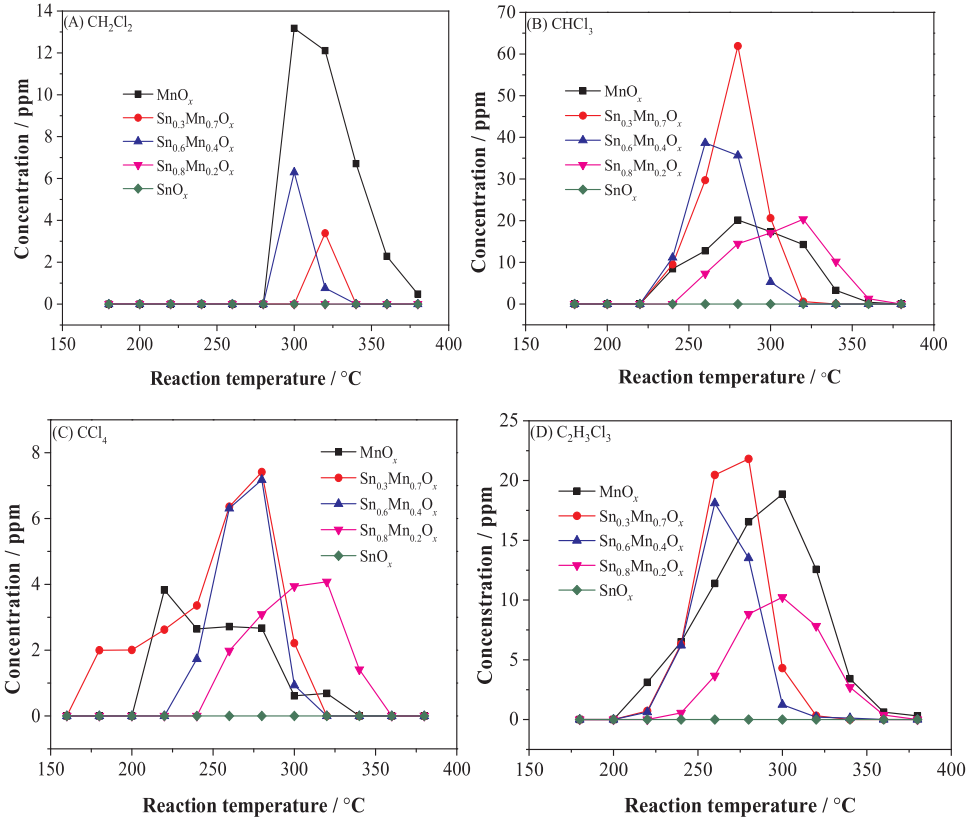

Fig. 7. Concentration of byproducts (A) CH_2Cl_2, (B) $CHCl_3$, (C) CCl_4 and (D) $C_2H_3Cl_3$ as a function of reaction temperature over $Sn_yMn_{1-y}O_x$ (y = 0, 0.3, 0.6, 0.8 and 1.0) catalysts.

VC conversion of the step over different catalysts.

3.8. Byproducts analysis

It was reported that chlorinated organics were usually produced as the main byproducts in the catalytic oxidation of CVOCs [51,52], thus it is essential to analyze the chemical compositions in the effluent of VC oxidation, especially the Cl-containing organics. Herein, it was detected that the main byproducts were dichloromethane (CH_2Cl_2), trichloromethane ($CHCl_3$), tetrachloromethane (CCl_4) and 1,1,2-trichloroethane (CH_2Cl-$CHCl_2$), and their concentrations as a function of reaction temperature are illustrated in Fig. 7. Over pure SnO_2, no byproduct was observed in the reaction temperature range. In contrary, the chlorinated byproducts of CH_2Cl_2, $CHCl_3$, CCl_4 and CH_2Cl-$CHCl_2$ were formed over pure MnO_x, and the concentration of all four byproducts increased firstly and then decreased with an increase in the reaction temperature from 175 to 380 °C. On the whole, $CHCl_3$ and CH_2Cl-$CHCl_2$ accounted for the high proportion while the proportion of CCl_4 was almost negligible. With addition of Sn into pure MnO_x, the four byproducts mentioned above were also observed and the corresponding proportion was dependent on the Sn/Mn molar ratio of $Sn_yMn_{1-y}O_x$ catalysts. The concentration of CH_2Cl_2 decreased obviously over $Sn_yMn_{1-y}O_x$ catalysts compared with that over pure MnO_x. In contrary, the concentrations of $CHCl_3$ and CCl_4 increased to some extent. As a result, among the four byproducts, $CHCl_3$ was dominant and the highest concentration of $CHCl_3$ over $Sn_yMn_{1-y}O_x$ catalysts varied in the range of 20–62 ppm. Meanwhile, CH_2Cl-$CHCl_2$, the second largest percentage in byproducts, reached the maximum of 10–22 ppm over $Sn_yMn_{1-y}O_x$ catalysts.

It is proposed [53] that CH_2Cl-$CHCl_2$ can be produced by the chlorine addition reaction of vinyl chloride, and then be catalytically cracked into CH_2Cl_2 and $CHCl_3$ via thermal decomposition. Finally, CCl_4 could be originated from further chlorination of $CHCl_3$.Over $Sn_{0.6}Mn_{0.4}O_x$ catalyst, the major chlorinated byproducts of $CHCl_3$ and CH_2Cl-$CHCl_2$ were initially formed at 220 °C and reached the maximum of 38 and 18 ppm at 260–280 °C, respectively. Besides, relatively lower amounts of CH_2Cl_2 and CCl_4 were detected at 220–340 °C. All the four byproducts can be completely eliminated below 340 °C, lower than other catalysts, due to its high catalytic activity at low temperature.

3.9. Catalytic stability and effect of water

The stability of $Sn_{0.6}Mn_{0.4}O_x$ catalyst for VC oxidation was carried out at the reaction temperature of 265, 300 and 340 °C for 100 h, respectively. As shown in Fig. 8, VC conversion of $Sn_{0.6}Mn_{0.4}O_x$ catalyst

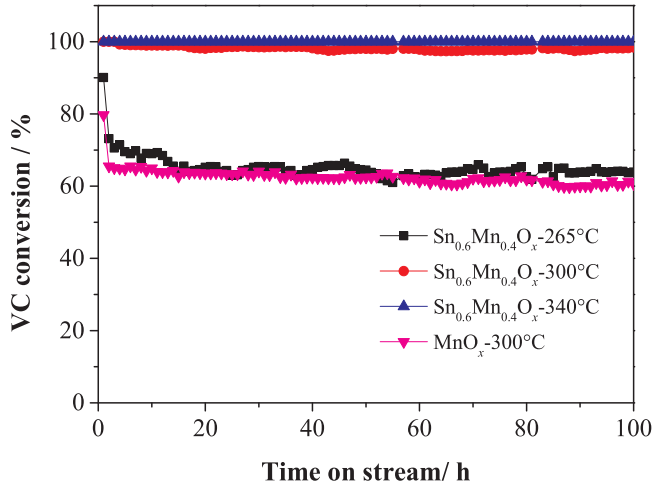

Fig. 8. VC conversion as a function of time on stream over $Sn_{0.6}Mn_{0.4}O_x$ and MnO_x catalysts.

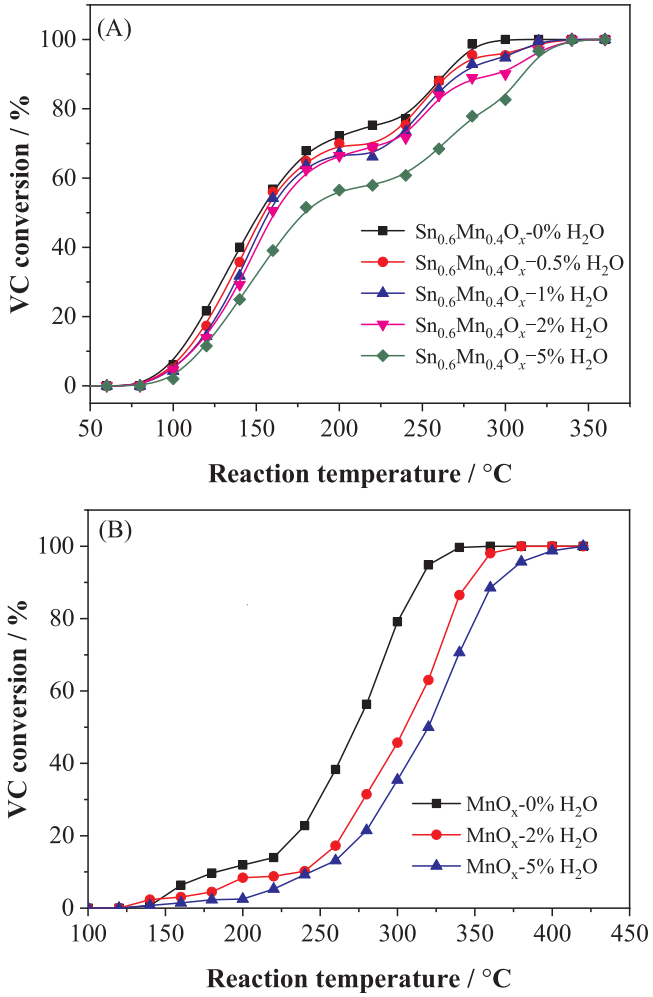

Fig. 9. VC conversion as a function of reaction temperature over (A) $Sn_{0.6}Mn_{0.4}O_x$ catalyst with 0.5 vol%, 1 vol%, 2 vol% and 5 vol% water, (B) pure MnO_x catalyst with 2 vol% and 5 vol% water.

decreased obviously from 90% to 70% during the first 3 h at 265 °C, which was attributed to the accumulation of Cl species on the catalyst surface and the coverage of active sites, confirmed by XPS results (Fig. S1 and Table S1). Afterwards, VC conversion decreased slowly to about 64% at the following 12 h and then maintained stable for 85 h. When the stability testing was performed at higher reaction temperatures, i.e., 300 and 340 °C, $Sn_{0.6}Mn_{0.4}O_x$ catalyst exhibited excellent catalytic stability with VC conversion of 98% and 100% within 100 h, respectively. More importantly, no chlorinated byproducts were observed at 340 °C. In contrary, when reacting at 300 °C over pure MnO_x catalyst, VC conversion declined rapidly in the first hour, and then decreased gently to 60% in the flowing 99 h. It means that Cl desorption is still a difficult process over pure MnO_x even at 300 °C. These results indicate that $Sn_{0.6}Mn_{0.4}O_x$ catalyst exhibits excellent catalytic stability for VC oxidation in low reaction temperature.

On the other hand, as required for the practical applications of the catalysts, water inevitably exists in the industrial effluents, which may quickly poison the catalysts. Therefore, it is necessary to investigate effect of water on the catalytic activity of $Sn_{0.6}Mn_{0.4}O_x$ and MnO_x catalysts for VC oxidation, respectively. Fig. 9A shows VC conversion over $Sn_{0.6}Mn_{0.4}O_x$ catalyst under the reactant gas containing 0.5 vol.%, 1 vol.%, 2 vol.% and 5 vol.% water, respectively. It was noted that the catalytic activity of $Sn_{0.6}Mn_{0.4}O_x$ catalyst did not change significantly under the reactant gases containing 0.5 vol.%, 1 vol.% and 2 vol.% water. However, when the water content in the reactant gas reached

5 vol.%, the catalytic activity of $Sn_{0.6}Mn_{0.4}O_x$ catalyst significantly reduced, in which T_{50} and T_{90} was 180 and 311 °C, 28 and 47 °C higher than those under the dry reactant gas, respectively. The decrease in the catalytic activity of $Sn_{0.6}Mn_{0.4}O_x$ catalyst under 5 vol.% H_2O may be due to the competitive adsorption of H_2O with VC on the active sites [54]. In contrary, VC conversion markedly decreased over pure MnO_x catalyst under the reactant gas containing 2 vol.% and 5 vol.% water, which is shown in Fig. 9B. It means that the water-resistant performance of pure MnO_x catalyst is greatly improved with addition of Sn.

4. Discussion

In general, catalytic combustion of vinyl chloride can be divided into two steps. The first one is the dechlorination reaction. Considering the conjugation between the unshared electron pairs of the chlorine atom and the C=C double bond, the C−Cl bond of VC is relatively stable, and the dechlorination reaction is not easy to occur. Therefore, the acids sites of the catalysts may play a key role in the dechlorination reaction, especially Lewis acids sites. The electron-withdrawing effect of Lewis acids may weaken the conjugation effect between the C−Cl and the C=C double bond, which makes the dechlorination reaction occur in lower reaction temperature. The second step is the oxidation of $-C_2H_3$, which is completely dependent on the redox property. Therefore, an efficient catalyst for VC oxidation should possess plenty of acids sites and excellent redox property.

Herein, a series of Sn-Mn composite oxides with different Sn/Mn molar ratios were prepared by a co-precipitation method. The XRD results reveal that addition of Sn can significantly reduce the crystallization of pure MnO_x due to the formation of Sn-Mn-O solid solution. Furthermore, SnO_2 phase exists in $Sn_{0.3}Mn_{0.7}O_x$ catalyst besides Sn-Mn-O solid solution. With the Sn/Mn molar ratio increases to 0.6/0.4 and 0.8/0.2, the catalysts only exhibit the diffraction peaks assigned to rutile SnO_2 due to the formation of Sn-Mn-O solid solution, in which Mn^{4+} or Mn^{3+} is incorporated into the SnO_2 lattice. As a result, the surface area of $Sn_yMn_{1-y}O_x$ catalyst significantly increases in comparsion with that of pure MnO_x. On the other hand, as shown in XPS results, addition of Sn into pure MnO_x can prompt the existence of Mn with high valence states. The Mn^{4+}/Mn^{3+} ratios increase to 0.86 and 0.88 over $Sn_{0.6}Mn_{0.4}O_x$ and $Sn_{0.8}Mn_{0.2}O_x$ catalysts, compared with 0.43 over pure MnO_x. Meanwhile, the O_β (surface oxygen species)/O_α (lattice oxygen species) ratios on the surface of $Sn_yMn_{1-y}O_x$ catalysts also increase compared with pure SnO_x and MnO_x, which indicates that Sn-Mn-O solid solution possesses more surface active oxygen species. High valence states of Mn and more surface active oxygen species are propitious to improvement of the oxidation ability of $Sn_yMn_{1-y}O_x$ catalysts.

As for the redox property of $Sn_yMn_{1-y}O_x$ catalysts, based on the comprehensive consideration of the H_2 consumption amount and the temperature of the reduction peaks, $Sn_{0.3}Mn_{0.7}O_x$ and $Sn_{0.6}Mn_{0.4}O_x$ catalysts possess higher redox property compared with $Sn_{0.8}Mn_{0.2}O_x$ and pure MnO_x catalysts. Meanwhile, O_2-TPD indicates that neither physically adsorbed oxygen nor chemically adsorbed oxygen species exist over pure MnO_x and SnO_x catalysts. In contrary, chemically adsorbed oxygen species exist over $Sn_yMn_{1-y}O_x$ catalysts due to the formation of Sn-Mn-O solid solution. Furthermore, the amount of chemically adsorbed oxygen species is in the order: $Sn_{0.6}Mn_{0.4}O_x > Sn_{0.3}Mn_{0.7}O_x \gg Sn_{0.8}Mn_{0.2}O_x$, and $Sn_{0.6}Mn_{0.4}O_x$ catalyst possesses the most chemically adsorbed oxygen species. These above-mentioned results reveal that addition of Sn can significantly enhance the redox ability of MnO_x, and $Sn_{0.6}Mn_{0.4}O_x$ catalyst is the best.

The surface acidity of the catalysts was investigated by NH_3-TPD. The results indicate that with introduction of Sn into pure MnO_x, the amount of acids sites increases significantly compared with pure MnO_x, principally weak and medium acid sites, due to the formation of Sn-Mn-O solid solution. The amount of weak and medium adsorbed NH_3 is in the order: $Sn_{0.6}Mn_{0.4}O_x > Sn_{0.3}Mn_{0.7}O_x > Sn_{0.8}Mn_{0.2}O_x \gg MnO_x$, and $Sn_{0.6}Mn_{0.4}O_x$ possesses the most weak and medium acid sites.

Above all, addition of Sn can increase the surface acid and redox property of pure MnO_x. Furthermore, the Sn/Mn molar ratio of $Sn_yMn_{1-y}O_x$ catalyst significantly affects these two properties, among which $Sn_{0.6}Mn_{0.4}O_x$ catalyst possesses the most amount of surface acids sites and the most excellent redox property. According to the catalytic reaction mechanism of vinyl chloride combustion, these factors significantly improve the catalytic activity of $Sn_yMn_{1-y}O_x$ catalyst. Therefore, as might be expected, the catalytic activity of $Sn_yMn_{1-y}O_x$ catalyst is higher than those of pure MnO_x and SnO_2 catalysts, and $Sn_{0.6}Mn_{0.4}O_x$ catalyst exhibits the best catalytic activity for VC combustion with the corresponding E_a of 49.8 kJ/mol. More exciting, $Sn_{0.6}Mn_{0.4}O_x$ catalyst can oxidize VC completely without any chlorinated byproducts at low reaction temperature of 340 °C.

5. Conclusions

$Sn_yMn_{1-y}O_x$ composite oxide catalysts with different Sn/Mn ratios were prepared by a co-precipitation method. Based on the formation of Sn-Mn-O solid solution structure, compared with pure SnO_x and MnO_x catalysts, $Sn_yMn_{1-y}O_x$ catalysts exhibit higher redox property and ability to adsorb oxygen due to the presence of more Mn^{4+} species and surface adsorbed oxygen species. What is more, $Sn_yMn_{1-y}O_x$ catalysts have more weak and medium acid sites on the catalyst surface. Therefore, the catalytic activity of $Sn_yMn_{1-y}O_x$ catalysts for the catalytic combustion of VC is significantly improved compared with pure SnO_x and MnO_x catalysts. Moreover, among $Sn_yMn_{1-y}O_x$ catalysts with different Sn/Mn ratios, these promoting effects are the most obvious over $Sn_{0.6}Mn_{0.4}O_x$ catalyst, which leads to the best catalytic activity for VC combustion at the reaction temperature of 340 °C without any chlorinated byproducts. Meanwhile, $Sn_{0.6}Mn_{0.4}O_x$ catalyst exhibits excellent catalytic stability for 100 h and high water-resisting ability. We hope that this work will exemplify a promising strategy for developing efficient MnO_x-based catalysts for the catalytic combustion of chlorohydrocarbons.

Acknowledgements

This work was supported by the National Key Research and Development Program of China (2016YFC0204300), the National Natural Science Foundation of China (21577035), the Commission of Science and Technology of Shanghai Municipality (15DZ1205305), and the Fundamental Research Funds for the Central Universities (222201717003).

Appendix A. Supplementary data

Supplementary material related to this article can be found, in the online version, at doi:https://doi.org/10.1016/j.apcatb.2019.117748.

References

[1] B.M. Weckhuysen, G. Mestl, M.P. Rosynek, T.R. Krawietz, J.F. Haw, J.H. Lunsford, Destructive adsorption of carbon tetrachloride on alkaline earth metal oxides, J. Phys. Chem. B 102 (1998) 3773–3778.
[2] J.I. Gutiérrez-Ortiz, B. de Rivas, R. López-Fonseca, J.R. González-Velasco, Catalytic purification of waste gases containing VOC mixtures with Ce/Zr solid solutions, Appl. Catal. B: Environ. 65 (2006) 191–200.
[3] Z. Hu, S. Qiu, Y. You, Y. Guo, Y. Guo, L. Wang, W. Zhan, G. Lu, Hydrothermal synthesis of $NiCeO_x$ nanosheets and its application to the total oxidation of propane, Appl. Catal. B: Environ. 225 (2018) 110–120.
[4] Z. Hu, Z. Wang, Y. Guo, L. Wang, Y. Guo, J. Zhang, W. Zhan, Total oxidation of propane over a Ru/CeO_2 catalyst at low temperature, Environ. Sci. Technol. 52 (2018) 9531–9541.
[5] C. Zhang, H. Huang, G. Li, L. Wang, L. Song, X. Li, Zeolitic acidity as a promoter for the catalytic oxidation of toluene over MnO_x/HZSM-5 catalysts, Catal. Today 327 (2019) 374–381.
[6] G. Li, C. Zhang, Z. Wang, H. Huang, H. Peng, X. Li, Fabrication of mesoporous Co_3O_4 oxides by acid treatment and their catalytic performances for toluene oxidation, Appl. Catal. A Gen. 550 (2018) 67–76.
[7] X. Ma, Q. Sun, X. Feng, X. He, J. Guo, H. Sun, H. Cao, Catalytic oxidation of 1,2-

dichlorobenzene over $CaCO_3$/α-Fe_2O_3 nanocomposite catalysts, Appl. Catal. A Gen. 450 (2013) 143–151.
[8] T. Cai, H. Huang, W. Deng, Q. Dai, W. Liu, X. Wang, Catalytic combustion of 1,2-dichlorobenzene at low temperature over Mn-modified Co_3O_4 catalysts, Appl. Catal. B: Environ. 166–167 (2015) 393–405.
[9] B. de Rivas, R. López-Fonseca, M.A. Gutiérrez-Ortiz, J.I. Gutiérrez-Ortiz, Impact of induced chlorine-poisoning on the catalytic behaviour of $Ce_{0.5}Zr_{0.5}O_2$ and $Ce_{0.15}Zr_{0.85}O_2$ in the gas-phase oxidation of chlorinated VOCs, Appl. Catal. B: Environ. 104 (2011) 373–381.
[10] B.H. Aristizabal, C. Montes de Correa, A.I. Serykh, C.E. Hetrick, M.D. Amiridis, In situ FTIR study of the adsorption and reaction of ortho-dichlorobenzene on Pd–Co sulfated zirconia catalysts, J. Catal. 258 (2008) 95–102.
[11] A. Aranzabal, J.A. González-Marcos, M. Romero-Sáez, J.R. González-Velasco, M. Guillemot, P. Magnoux, Stability of protonic zeolites in the catalytic oxidation of chlorinated VOCs (1,2-dichloroethane), Appl. Catal. B: Environ. 88 (2009) 533–541.
[12] J.I. Gutiérrez-Ortiz, R. López-Fonseca, U. Aurrekoetxea, J.R. González-Velasco, Low-temperature deep oxidation of dichloromethane and trichloroethylene by H-ZSM-5-supported manganese oxide catalysts, J. Catal. 218 (2003) 148–154.
[13] R. López-Fonseca, B. de Rivas, J.I. Gutiérrez-Ortiz, A. Aranzabal, J.R. González-Velasco, Enhanced activity of zeolites by chemical dealumination for chlorinated VOC abatement, Appl. Catal. B: Environ. 41 (2003) 31–42.
[14] W. Zhao, J. Cheng, L. Wang, J. Chu, J. Qu, Y. Liu, S. Li, H. Zhang, J. Wang, Z. Hao, T. Qi, Catalytic combustion of chlorobenzene on the Ln modified Co/HMS, Appl. Catal. B: Environ. 127 (2012) 246–254.
[15] I. Maupin, L. Pinard, J. Mijoin, P. Magnoux, Bifunctional mechanism of dichloromethane oxidation over Pt/Al_2O_3: CH_2Cl_2 disproportionation over alumina and oxidation over platinum, J. Catal. 291 (2012) 104–109.
[16] R. Ma, P. Hu, L. Jin, Y. Wang, J. Lu, M. Luo, Characterization of CrO_x/Al_2O_3 catalysts for dichloromethane oxidation, Catal. Today 175 (2011) 598–602.
[17] X. Wang, Q. Kang, D. Li, Catalytic combustion of chlorobenzene over MnO_x–CeO_2 mixed oxide catalysts, Appl. Catal. B: Environ. 86 (2009) 166–175.
[18] D.A. Aguilera, A. Perez, R. Molina, S. Moreno, Cu–Mn and Co–Mn catalysts synthesized from hydrotalcites and their use in the oxidation of VOCs, Appl. Catal. B: Environ. 104 (2011) 144–150.
[19] M.S. Kamal, S.A. Razzak, M.M. Hossain, Catalytic oxidation of volatile organic compounds (VOCs) – a review, Atmos. Environ. 140 (2016) 117–134.
[20] C. Zhang, C. Wang, S. Gil, A. Boreave, L. Retailleau, Y. Guo, J.L. Valverde, A. Giroir-Fendler, Catalytic oxidation of 1,2-dichloropropane over supported $LaMnO_x$ oxides catalysts, Appl. Catal. B: Environ. 201 (2017) 552–560.
[21] M. Wu, X. Wang, Q. Dai, Y. Gu, D. Li, Low temperature catalytic combustion of chlorobenzene over Mn–Ce–O/γ-Al_2O_3 mixed oxides catalyst, Catal. Today 158 (2010) 336–342.
[22] X. Wang, L. Ran, Y. Dai, Y. Lu, Q. Dai, Removal of Cl adsorbed on Mn–Ce–La solid solution catalysts during CVOC combustion, J. Colloid Interface Sci. 426 (2014) 324–332.
[23] H. Li, G. Lu, Q. Dai, Y. Wang, Y. Guo, Y. Guo, Efficient low-temperature catalytic combustion of trichloroethylene over flower-like mesoporous Mn-doped CeO_2 microspheres, Appl. Catal. B: Environ. 102 (2011) 475–483.
[24] C. Zhang, C. Wang, W. Hua, Y. Guo, G. Lu, S. Gil, A. Giroir-Fendler, Relationship between catalytic deactivation and physicochemical properties of $LaMnO_3$ perovskite catalyst during catalytic oxidation of vinyl chloride, Appl. Catal. B: Environ. 186 (2016) 173–183.
[25] Ç. Kılıç, A. Zunger, Origins of coexistence of conductivity and transparency in SnO_2, Phys. Rev. Lett. 88 (2002) 095501.
[26] G. Zhang, W. Han, H. Zhao, L. Zong, Z. Tang, Solvothermal synthesis of well-designed ceria-tin-titanium catalysts with enhanced catalytic performance for wide temperature NH_3-SCR reaction, Appl. Catal. B: Environ. 226 (2018) 117–126.
[27] Q. Sun, X. Xu, H. Peng, X. Fang, W. Liu, J. Ying, F. Yu, X. Wang, SnO_2-based solid solutions for CH_4 deep oxidation: quantifying the lattice capacity of SnO_2 using an X-ray diffraction extrapolation method, Chin. J. Catal. 37 (2016) 1293–1302.
[28] X. Xu, R. Zhang, X. Zeng, X. Han, Y. Li, Y. Liu, X. Wang, Effects of La, Ce, and Y oxides on SnO_2 catalysts for CO and CH_4 oxidation, ChemCatChem 5 (2013) 2025–2036.
[29] X. Xu, F. Liu, X. Han, Y. Wu, W. Liu, R. Zhang, N. Zhang, X. Wang, Elucidating the promotional effects of niobia on SnO_2 for CO oxidation: developing an XRD extrapolation method to measure the lattice capacity of solid solutions, Catal. Sci. Technol. 6 (2016) 5280–5291.
[30] X. Wang, Y. Xie, Total oxidation of CH_4 on Sn-Cr composite oxide catalysts, Appl. Catal. B: Environ. 35 (2001) 85–94.
[31] Z. Hao, Y. Jiao, Q. Shi, H. Zhang, S. Zhan, Improvement of NH_3-SCR performance and SO_2 resistance over Sn modified $CeMoO_x$ electrospun fibers at low temperature, Catal. Today 327 (2019) 37–46.
[32] Z. Liu, X. Feng, Z. Zhou, Y. Feng, J. Li, Ce-Sn binary oxide catalyst for the selective catalytic reduction of NO_x by NH_3, Appl. Surf. Sci. 428 (2018) 526–533.
[33] X. Li, Y. Li, S. Deng, T.A. Rong, A Ce–Sn–O_x catalyst for the selective catalytic reduction of NO_x with NH_3, Catal. Commun. 40 (2013) 47–50.
[34] F. Wang, H. Dai, J. Deng, G. Bai, K. Ji, Y. Liu, Manganese oxides with rod-, wire-, tube-, and flower-like morphologies: highly effective catalysts for the removal of toluene, Environ. Sci. Technol. 46 (2012) 4034–4041.
[35] S. Ponce, M.A. Peña, J.L.G. Fierro, Surface properties and catalytic performance in methane combustion of Sr-substituted lanthanum manganites, Appl. Catal. B: Environ. 24 (2000) 193–205.
[36] D.A. Peña, B.S. Uphade, P.G. Smirniotis, TiO_2-supported metal oxide catalysts for low-temperature selective catalytic reduction of NO with NH_3: I. Evaluation and characterization of first row transition metals, J. Catal. 221 (2004) 421–431.
[37] D. Meng, Q. Xu, Y. Jiao, Y. Guo, Y. Guo, L. Wang, G. Lu, W. Zhan, Spinel structured $Co_aMn_bO_x$ mixed oxide catalyst for the selective catalytic reduction of NOx with NH_3, Appl. Catal. B: Environ. 221 (2018) 652–663.
[38] D. Meng, W. Zhan, Y. Guo, Y. Guo, Y. Wang, L. Wang, G. Lu, A highly effective catalyst of Sm-Mn mixed oxide for the selective catalytic reduction of NO_x with ammonia: effect of the calcination temperature, J. Mol. Catal. A Chem. 420 (2016) 272–281.
[39] D. Meng, W. Zhan, Y. Guo, Y. Guo, L. Wang, G. Lu, A highly effective catalyst of Sm-MnO_x for the NH_3-SCR of NO_x at low temperature: promotional role of Sm and its catalytic performance, ACS Catal. 5 (2015) 5973–5983.
[40] C. Zhang, C. Wang, H. Huang, K. Zeng, Z. Wang, H.-p. Jia, X. Li, Insights into the size and structural effects of zeolitic supports on gaseous toluene oxidation over MnO_x/HZSM-5 catalysts, Appl. Surf. Sci. 486 (2019) 108–120.
[41] A. Machocki, T. Ioannides, B. Stasinska, W. Gac, G. Avgouropoulos, D. Delimaris, W. Grzegorczyk, S. Pasieczna, Manganese-lanthanum oxides modified with silver for the catalytic combustion of methane, J. Catal. 227 (2004) 282–296.
[42] C. Zhang, C. Wang, W. Zhan, Y. Guo, Y. Guo, G. Lu, A. Baylet, A. Giroir-Fendler, Catalytic oxidation of vinyl chloride emission over $LaMnO_3$ and $LaB_{0.2}Mn_{0.8}O_3$ (B = Co, Ni, Fe) catalysts, Appl. Catal. B: Environ. 129 (2013) 509–516.
[43] L. Jing, H. Fu, B. Wang, D. Wang, B. Xin, S. Li, J. Sun, Effects of Sn dopant on the photoinduced charge property and photocatalytic activity of TiO_2 nanoparticles, Appl. Catal. B: Environ. 62 (2006) 282–291.
[44] N.S. Ramgir, I.S. Mulla, K.P. Vijayamohanan, Effect of RuO_2 in the shape selectivity of submicron-sized SnO_2 structures, J. Phys. Chem. B 109 (2005) 12297–12303.
[45] M.R. Morales, B.P. Barbero, L.E. Cadús, Combustion of volatile organic compounds on manganese iron or nickel mixed oxide catalysts, Appl. Catal. B: Environ. 74 (2007) 1–10.
[46] L. Cheng, Y. Men, J. Wang, H. Wang, W. An, Y. Wang, Z. Duan, J. Liu, Crystal facet-dependent reactivity of α-Mn_2O_3 microcrystalline catalyst for soot combustion, Appl. Catal. B: Environ. 204 (2017) 374–384.
[47] R. Sasikala, N.M. Gupta, S.K. Kulshreshtha, Temperature-programmed reduction and CO oxidation studies over Ce–Sn mixed oxides, Catal. Lett. 71 (2001) 69–73.
[48] C. Liu, H. Xian, Z. Jiang, L. Wang, J. Zhang, L. Zheng, Y. Tan, X. Li, Insight into the improvement effect of the Ce doping into the SnO_2 catalyst for the catalytic combustion of methane, Appl. Catal. B: Environ. 176–177 (2015) 542–552.
[49] Y. Xie, Y. Guo, Y. Guo, L. Wang, W. Zhan, Y. Wang, X. Gong, G. Lu, A highly-efficient La-MnO_x catalyst for propane combustion: the promotional role of La and the effect of the preparation method, Catal. Sci. Technol. 6 (2016) 8222–8233.
[50] Q. Dai, W. Wang, X. Wang, G. Lu, Sandwich-structured CeO_2@ZSM-5 hybrid composites for catalytic oxidation of 1, 2-dichloroethane: an integrated solution to coking and chlorine poisoning deactivation, Appl. Catal. B: Environ. 203 (2017) 31–42.
[51] B. de Rivas, N. Guillén-Hurtado, R. López-Fonseca, F. Coloma-Pascual, A. García-García, J.I. Gutiérrez-Ortiz, A. Bueno-López, Activity, selectivity and stability of praseodymium-doped CeO_2 for chlorinated VOCs catalytic combustion, Appl. Catal. B: Environ. 121–122 (2012) 162–170.
[52] C. Wang, C. Zhang, W. Hua, Y. Guo, G. Lu, S. Gil, A. Giroir-Fendler, Low-temperature catalytic oxidation of vinyl chloride over Ru modified Co_3O_4 catalysts, RSC Adv. 6 (2016) 99577–99585.
[53] W. Deng, Q. Dai, Y. Lao, B. Shi, X. Wang, Low temperature catalytic combustion of 1,2-dichlorobenzene over CeO_2-TiO_2 mixed oxide catalysts, Appl. Catal. B: Environ. 181 (2016) 848–861.
[54] Q. Dai, S. Bai, X. Wang, G. Lu, Catalytic combustion of chlorobenzene over Ru-doped ceria catalysts: mechanism study, Appl. Catal. B: Environ. 129 (2013) 580–588.